Research Article

C^1 Hermite Interpolation with PH Curves Using the Enneper Surface

Hyun Chol Lee,[1] Jae Hoon Kong,[1] and Gwangil Kim (iD) **[1,2]**

[1]*Department of Mathematics, Gyeongsang National University, Jinju 660-701, Republic of Korea*
[2]*Research Institute of Natural Science, Gyeongsang National University, Jinju 660-701, Republic of Korea*

Correspondence should be addressed to Gwangil Kim; gikim@gnu.ac.kr

We show that the geometric and PH-preserving properties of the Enneper surface allow us to find PH interpolants for all regular C^1 Hermite data-sets. Each such data-set is satisfied by two scaled Enneper surfaces, and we can obtain four interpolants on each surface. Examples of these interpolants were found to be better, in terms of bending energy and arc-length, than those obtained using a previous PH-preserving mapping.

1. Introduction

Pythagorean-hodograph (PH) curves were first introduced by Farouki and Sakkalis [1] as polynomial curves in $\mathbb{R}^2$ with polynomial speed functions, which have polynomial arc-lengths, rational curvature functions, and rational offsets, all of which derive from their polynomial speed functions. These properties make PH curves good candidates for CAGD and CAD/CAM applications such as interpolation of discrete data and control of motion along curved paths [2–4]. Also, these PH curves have subsequently been extended, with several applications, to rational curves with rational speed functions in $\mathbb{R}^n$ [3, 5, 6].

PH curves have been the subject of a great deal of study, both their formal representation [7–9] and their practical applications [7–11]. PH curves have been generalized [11] to participate in medial axis transforms [3, 12], becoming MPH curves in the Minkowski space $\mathbb{R}^{m,1}$ [8, 13, 14], and this has motivated a lot of further research. There has also been a lot of work on the use of PH curves for interpolating planar [7, 8, 10, 15, 16] and spatial data-sets [17–21], in particular to meet G^1 Hermite [20, 22, 23] and C^2 Hermite conditions [7]. In particular, C^1 Hermite interpolation problems have been solved by several techniques [13, 24–27] including PH-preserving mappings [24], which have recently been extended [13] to MPH-preserving mappings.

In this paper, we show that we can use Enneper surfaces to solve C^1 Hermite interpolation problems with PH curves, by exploiting two properties of the Enneper surface: the geometric property that it contains two straight lines and the PH-preserving nature of its parametrization. Since Farouki and Neff's original work on C^1 Hermite interpolation with PH curves, there have been many developments: in particular, it has been shown [24] that C^1 Hermite interpolation problems with PH curves in $\mathbb{R}^3$ can be reduced to problems in $\mathbb{R}^2$ and generic interpolants can then be obtained to satisfy a given C^1 Hermite data-set. This is achieved by a special cubic PH-preserving mapping which satisfies the data-set. However, significant drawbacks remain with this method: one is that the algebraic manipulations required are long and complicated; and the other is that this method is restricted to a special class of C^1 Hermite data-sets. We will address both of these issues: using the Enneper surface, we can solve C^1 Hermite interpolation problems more efficiently for all regular C^1 Hermite data-sets; and we will show that the interpolants obtained by this method may be expected to have better shapes than those obtained by the special mapping, in terms of both bending energy and arc-length.

The rest of this paper is organized as follows: In Section 2, we define the Pythagorean-hodograph curve and the PH-preserving mapping and give examples. In Section 3, we show that the parametrization of the Enneper surface in standard

form is PH-preserving and that, by rescaling the Enneper surface, we can find two cubic surfaces that satisfy any regular C^1 Hermite data-set. We also prove that we can obtain eight interpolants on the two cubic surfaces that satisfy a regular C^1 Hermite data-set. In Section 4, we compare our method with the use of PH-preserving cubic mappings [24], from two different perspectives: the amount of algebraic computation required and the geometric characterizations of the resulting curves. By empirical comparison of interpolants for the same data-set, we show that our method is more efficient and stable than the use of mappings. In Section 5, we summarize the results of this work and propose some themes for further study.

2. Preliminary

Let $\mathbb{R}^n$ be the n-dimensional Euclidean space, for $n \in \mathbb{N}$, and let $\mathbb{P}[t]$ be the set of polynomial functions with real coefficients. We express a polynomial curve in $\mathbb{R}^n$ as a mapping $\mathbf{r} : \mathbb{R} \rightarrow \mathbb{R}^n$ from the space of real numbers $\mathbb{R}$ to $\mathbb{R}^n$, such that the component functions of $\mathbf{r}$, which are $x_1(t), x_2(t), \ldots, x_n(t)$, are members of $\mathbb{P}[t]$.

Definition 1. A polynomial curve $\mathbf{r}(t) = (x_1(t), x_2(t), \ldots, x_n(t))$ is said to be a *Pythagorean-hodograph (PH)* curve if its velocity vector or hodograph $\mathbf{r}'(t) = (x_1'(t), \ldots, x_n'(t))$ satisfies the Pythagorean condition

$$\left\| \mathbf{r}'(t) \right\|_n^2 = x_1'(t)^2 + x_2'(t)^2 + \cdots + x_n'(t)^2 = \sigma(t)^2, \quad (1)$$

where $\| * \|_n$ denotes the Euclidean norm of $\mathbb{R}^n$ and $\sigma(t) \in \mathbb{P}[t]$.

Definition 2. A polynomial mapping $\phi : \mathbb{R}^n \rightarrow \mathbb{R}^m$ is said to be *PH-preserving* if, for every PH curve $\mathbf{r}(t)$ in $\mathbb{R}^n$, $\phi(\mathbf{r}(t))$ is a PH curve in $\mathbb{R}^m$.

Example 3. Let Ψ be an affine transformation given by

$$\Psi(\mathbf{p}) = \lambda \mathbf{R} \mathbf{p} + \mathbf{k}, \quad \text{for } \forall \mathbf{p} \in \mathbb{R}^3, \quad (2)$$

where $\mathbf{R}$ is an orthogonal matrix in $\mathbb{R}^3$, $\lambda \in \mathbb{R} \setminus \{0\}$ is a scaling factor, and $\mathbf{k}$ is a constant vector in $\mathbb{R}^3$. Then, for a PH curve $\mathbf{r}(t) = (u(t), v(t))$ in $\mathbb{R}^2$, the mapping $\widetilde{\Psi} : \mathbb{R}^2 \rightarrow \mathbb{R}^3$ defined by

$$\widetilde{\Psi}(\mathbf{r}(t)) = \Psi(\mathbf{p}(t)), \quad \text{where } \mathbf{p}(t) = (u(t), v(t), 0) \quad (3)$$

is PH-preserving, since

$$\begin{aligned}
\left\| \widetilde{\Psi}(\mathbf{r}(t))' \right\|_3^2 &= \left\langle \widetilde{\Psi}(\mathbf{r}(t))', \widetilde{\Psi}(\mathbf{r}(t))' \right\rangle \\
&= \left\langle \lambda \mathbf{R} \mathbf{p}'(t), \lambda \mathbf{R} \mathbf{p}'(t) \right\rangle \\
&= \lambda^2 \left\langle \mathbf{p}'(t), \mathbf{p}'(t) \right\rangle = \lambda^2 \left\| \mathbf{p}'(t) \right\|_3^2 \\
&= \lambda^2 \left(u'(t)^2 + v'(t)^2 \right),
\end{aligned} \quad (4)$$

where $\langle , \rangle$ denotes the usual inner product in $\mathbb{R}^3$.

In addition, let $\mathscr{P}(u, v) = (x(u, v), y(u, v), z(u, v))$ be a polynomial mapping given by

$$\begin{aligned}
x(u, v) &= u^5 - 10u^3 v^2 + 5uv^4 + u^3 - 3uv^2, \\
y(u, v) &= v^5 - 10v^3 u^2 + 5vu^4 + v^3 - 3vu^2, \quad (5) \\
z(u, v) &= 2\sqrt{15} uv \left(u^2 - v^2 \right).
\end{aligned}$$

Then, for a $\mathbf{r}(t) = (u(t), v(t))$ in $\mathbb{R}^2$, since

$$\begin{aligned}
\frac{d}{dt} x(u(t), v(t)) = {} & 5u(t)^4 u'(t) - 30u(t)^2 v(t)^2 u'(t) \\
& - 20u(t)^3 v(t) v'(t) \\
& + 5v(t)^4 u'(t) \\
& + 20u(t) v(t)^3 v'(t) \\
& + 3u(t)^2 u'(t) - 3v(t)^2 u'(t) \\
& - 6u(t) v(t) v'(t),
\end{aligned} \quad (6)$$

$$\begin{aligned}
\frac{d}{dt} y(u(t), v(t)) = {} & 5v(t)^4 v'(t) - 30v(t)^2 u(t)^2 v'(t) \\
& - 20v(t)^3 u(t) u'(t) \\
& + 5u(t)^4 v'(t) \\
& + 20v(t) u(t)^3 u'(t) \\
& + 3v(t)^2 v'(t) - 3u(t)^2 v'(t) \\
& - 6u(t) v(t) u'(t),
\end{aligned} \quad (7)$$

$$\begin{aligned}
\frac{d}{dt} z(u(t), v(t)) = {} & 6\sqrt{15} u(t)^2 v(t) u'(t) \\
& + 2\sqrt{15} u(t)^3 v'(t) \\
& - 2\sqrt{15} v(t)^3 u'(t) \\
& - 6\sqrt{15} u(t) v(t)^2 v'(t),
\end{aligned} \quad (8)$$

we obtain

$$\begin{aligned}
\left\| \mathscr{P}(\mathbf{r}(t))' \right\|_3^2 &= \left(\frac{d}{dt} x(u(t), v(t)) \right)^2 \\
& + \left(\frac{d}{dt} y(u(t), v(t)) \right)^2 + \left(\frac{d}{dt} z(u(t), v(t)) \right)^2 \quad (9) \\
&= \left(u(t)^2 + v(t)^2 \right)^2 \left(5u(t)^2 + 5v(t)^2 + 3 \right)^2 \\
& \cdot \left(u'(t)^2 + v'(t)^2 \right).
\end{aligned}$$

This means that $\mathscr{P}(u, v)$ is PH-preserving. Figure 1(a) shows the image of $\mathscr{P}$ in $\mathbb{R}^3$, which is the PH-preserving surface parameterized by $\mathscr{P}$. The blue curve on the surface is the image of the curve $\gamma(t) = (t - (1/3)t^3, t^2)$ shown in Figure 1(b),
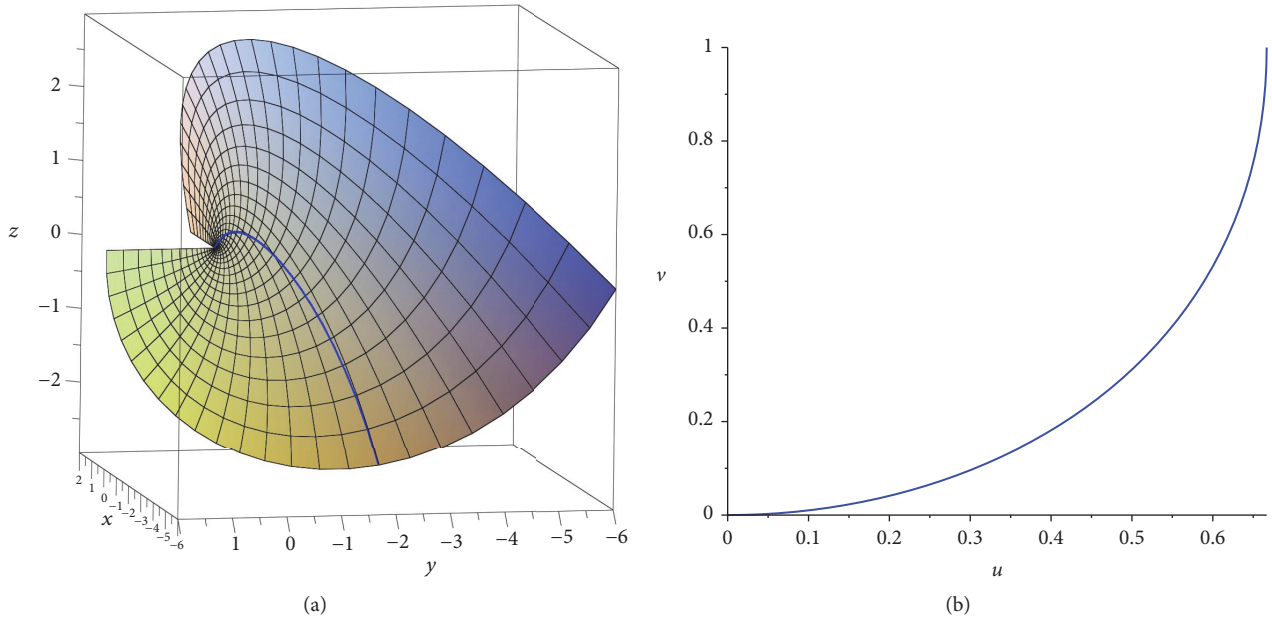
FIGURE 1: (a) A PH-preserving surface parameterized by $\mathscr{P}$, derived in Example 3, when $0 \leq t \leq 1$; the blue curve on the surface is the image of $\gamma(t)$, shown in (b).

which is a segment of the Tchirnhausen cubic. This is a PH curve in $\mathbb{R}^2$, and thus the curve on the surface is a PH curve in $\mathbb{R}^3$.

3. Construction of C^1 Hermite PH Interpolants on the Scaled Enneper Surface

Definition 4. Let $\Sigma \in \mathbb{R}^3$ be a surface with the parametrization $\Phi : \mathbb{R}^2 \to \mathbb{R}^3$ given by

$$\Phi(u, v) = \left(\frac{u^3}{3} - uv^2 + u, \frac{v^3}{3} - vu^2 + v, 2uv \right). \quad (10)$$

Σ is called the Enneper surface in standard form.

It is known [28] that PH curves in the domain of the Enneper surface can be mapped to PH curves on the surface: thus the parametrization of the Enneper surface is PH-preserving. We revisit this result briefly.

Theorem 5. Φ *is PH-preserving.*

Proof. Assume that $\mathbf{r}(t) = (u(t), v(t))$ is a PH curve in $\mathbb{R}^2$. Then, since

$$\left\| \Phi(\mathbf{r}(t))' \right\|_3^2 = \left(u(t)^2 u'(t) - u'(t) v(t)^2 \right.$$
$$- 2u(t) v(t) v'(t) + u'(t) \big)^2 + \left(v(t)^2 v'(t) \right.$$
$$- v'(t) u(t)^2 - 2v(t) u(t) u'(t) + v'(t) \big)^2$$
$$+ \left(2u'(t) v(t) + 2u(t) v'(t) \right)^2 = \left(u(t)^2 + v(t)^2 \right.$$

$$+ 1 \big)^2 \left(u'(t)^2 + v'(t)^2 \right), \quad (11)$$

the curve $\Phi(\mathbf{r}(t))$ in $\mathbb{R}^3$ is a PH curve. This completes the proof. $\square$

Theorem 6. Σ *contains two straight lines* $l_y = \{(x, y, z) \in \mathbb{R}^3 \mid x = 0, \ z = 0\}$ *and* $l_x = \{(x, y, z) \in \mathbb{R}^3 \mid y = 0, \ z = 0\}$ *on the xy-plane* $\{(x, y, z) \in \mathbb{R}^3 \mid z = 0\}$.

Proof. If $z(u, v) = 2uv = 0$, or equivalently $u = 0$ or $v = 0$, we immediately obtain $\Phi(0, v) = (0, v^3/3 + v, 0)$ or $\Phi(u, 0) = (u^3/3 + u, 0, 0)$. This completes the proof. $\square$

Remark 7. The Enneper surface is the nontrivial polynomial minimal surface of the lowest possible degree; equivalently it is area-minimizing, and the parametrization Φ is conformal (i.e., angle-preserving). Now we consider the surfaces obtained by rescaling the Enneper surface. Let Σ^λ be a polynomial surface of degree 3 given by the parametrization $\Phi^\lambda = \lambda\Phi$ where Φ is the standard parametrization of the Enneper surface and λ is a nonzero real number. Then Σ^λ is also a polynomial minimal surface of degree 3, and Φ^λ is PH-preserving, as shown in Example 3. From now on, we will call the surface Σ^λ the scaled Enneper surface (or s-Enneper surface) associated with a scaling factor λ. Note that all s-Enneper surfaces contain l_x and l_y, which we will use in Theorem 9.

Definition 8. A C^1 Hermite data-set $H_C^1 = \{\mathbf{p}_0, \mathbf{p}_1, \mathbf{v}_0, \mathbf{v}_1\}$ consists of two end-points $\mathbf{p}_0$ and $\mathbf{p}_1$, and two velocities $\mathbf{v}_0$

and $\mathbf{v}_1$ at those end-points, where $\mathbf{p}_0, \mathbf{p}_1, \mathbf{v}_0$ and $\mathbf{v}_1 \in \mathbb{R}^3$. H_C^1 is said to be *regular* if $\mathbf{p}_1 - \mathbf{p}_0, \mathbf{v}_0$ and $\mathbf{v}_1$ are linearly independent.

Also note that if $\mathbf{p}_0$ and $\mathbf{p}_1$ lie on a surface Σ, and $\mathbf{v}_0$ and $\mathbf{v}_1$ are tangents to that surface, then we can say that Σ satisfies H_C^1. If ϕ is a mapping which generates the surface Σ, then we can also say that ϕ satisfies H_C^1.

Theorem 9. *For a regular C^1 Hermite data-set $H_C^1 = \{(0,0,0),$ $(1,0,0), \mathbf{v}_0 = (v_{01}, v_{02}, 0),\ \mathbf{v}_1 = (v_{11}, v_{12}, v_{13})\}$, we can find two s-Enneper surfaces satisfying H_C^1.*

Proof. Let Σ^λ be the s-Enneper surface obtained by the parametrization $\Phi^\lambda = \lambda\Phi$ where Φ is the parametrization of the Enneper surface in standard form. First, since $\Phi^\lambda(0,0) = \lambda\Phi(0,0) = (0,0,0)$ for all $\lambda \in \mathbb{R} \setminus \{0\}$, it is obvious that $\mathbf{p}_0 = (0,0,0)$ lies on Σ^λ. In addition, as stated in Remark 7, by Theorem 5, we can find a point in l_x given by $(u_0^3/3 + u_0, 0, 0)$ and a suitable scaling factor λ, such that $\mathbf{p}_1 = (1,0,0) \in \Sigma^\lambda$: since $l_x \in \Sigma^\lambda$, we can assume the existence of some u_0 and λ such that

$$\Phi^\lambda(u_0, 0) = \lambda\Phi(u_0, 0) = \lambda\left(\frac{u_0^3}{3} + u_0, 0, 0\right). \quad (12)$$

Hence, if

$$\lambda = \frac{3}{u_0^3 + 3u_0} \quad \text{for some non-zero } u_0 \in \mathbb{R}, \quad (13)$$

we have $\Phi^\lambda(u_0, 0) = \mathbf{p}_1 = (1,0,0) \in \Sigma^\lambda$. That is, $\mathbf{p}_0 = (0,0,0)$ and $\mathbf{p}_1 = (1,0,0)$ lie on the s-Enneper surface parameterized by Φ^λ. Next we note that, since $\Phi_u^\lambda(0,0) = \lambda(1,0,0)$ and $\Phi_v^\lambda(0,0) = \lambda(0,1,0)$, the unit vector $\mathbf{n}_0$ normal to Σ^λ at $(0,0,0)$ is $(0,0,1)$. This means that $\langle\mathbf{n}_0, \mathbf{v}_0\rangle = 0$. Moreover, since

$$\begin{aligned}\Phi_u^\lambda(u_0, 0) &= \lambda\left(u_0^2 + 1, 0, 0\right),\\\Phi_v^\lambda(u_0, 0) &= \lambda\left(0, -u_0^2 + 1, 2u_0\right),\end{aligned} \quad (14)$$

we can obtain the unit vector $\mathbf{n}_1$ normal to Σ^λ at $(1,0,0)$ as follows:

$$\mathbf{n}_1 = \left(0, \frac{-2u_0}{1 + u_0^2}, \frac{1 - u_0^2}{1 + u_0^2}\right). \quad (15)$$

Here, since

$$\langle\mathbf{n}_1, \mathbf{v}_1\rangle = \frac{-2u_0}{1 + u_0^2}v_{12} + \frac{1 - u_0^2}{1 + u_0^2}v_{13}, \quad (16)$$

we can solve

$$v_{13}u_0^2 + 2v_{12}u_0 - v_{13} = 0 \quad (17)$$

when $v_{13} \neq 0$ and we obtain

$$u_0 = -\frac{v_{12}}{v_{13}} \pm \sqrt{1 + \left(-\frac{v_{12}}{v_{13}}\right)^2}. \quad (18)$$

Then, since the given data-set is regular, it is obvious that $v_{13} \neq 0$. Therefore $\mathbf{v}_0$ and $\mathbf{v}_1$ are tangent to the s-Enneper surface Σ^λ when

$$\begin{aligned}u_0 &= -\frac{v_{12}}{v_{13}} \pm \sqrt{1 + \left(-\frac{v_{12}}{v_{13}}\right)^2},\\\lambda &= \frac{3}{u_0^3 + 3u_0}.\end{aligned} \quad (19)$$

Consequently, Σ^λ satisfies H_C^1. This completes the proof. $\square$

Remark 10. Note that, if a data-set $H_C^1 = \{\mathbf{p}_0, \mathbf{p}_1, \mathbf{v}_0, \mathbf{v}_1\}$ is *not* regular, the three vectors $\mathbf{p}_1 - \mathbf{p}_0, \mathbf{v}_0$, and $\mathbf{v}_1$ must lie on the same plane. This means that the interpolation problem that must be solved to obtain PH curves satisfying the given data-set is equivalent to a planar C^1 Hermite interpolation, which has been studied thoroughly [3, 10, 15, 16], in parallel, including the case of solving the interpolation problem for such a data-set with MPH curves [14, 29, 30].

Example 11. Let $H_C^1 = \{(0,0,0), (1,0,0),\ \mathbf{v}_0 = (1,1,0),\ \mathbf{v}_1 = (2,1,2)\}$. Then, using Theorem 9, we can obtain the two s-Enneper surfaces shown in Figure 2: Figure 2(a) is the s-Enneper surface when $u_0 = (-1 + \sqrt{5})/2$ and $\lambda = (21 + 15\sqrt{5})/38$ and Figure 2(b) is the s-Enneper surface when $u_0 = (-1 - \sqrt{5})/2$ and $\lambda = (21 - 15\sqrt{5})/38$.

Theorem 12. *For a C^1 Hermite data-set $H_C^1 = \{(0,0,0),$ $(1,0,0), \mathbf{v}_0 = (v_{01}, v_{02}, 0), \mathbf{v}_1 = (v_{11}, v_{12}, v_{13})\}$, where $v_{13} \neq 0$. We can obtain four PH interpolants satisfying H_C^1 on each of the two s-Enneper surfaces which satisfy H_C^1.*

Proof. By Theorem 9, for $H_C^1 = \{(0,0,0), (1,0,0), \mathbf{v}_0 = (v_{01}, v_{02}, 0), \mathbf{v}_1 = (v_{11}, v_{12}, v_{13})\}$ with $v_{13} \neq 0$, we can obtain two s-Enneper surfaces satisfying H_C^1. Then, by using the parametrization Φ^λ of each s-Enneper surface, we can obtain a new C^1 Hermite data-set $\widetilde{H}_C^1 = \{\widetilde{\mathbf{p}}_0 = (0,0), \widetilde{\mathbf{p}}_1 = (u_0, 0),$ $\widetilde{\mathbf{v}}_0, \widetilde{\mathbf{v}}_1\}$ on $\mathbb{R}^2$ from the given H_C^1, which satisfies $\Phi^\lambda(0,0) = (0,0,0)$, $\Phi^\lambda(u_0, 0) = (1,0,0)$, $D\Phi^\lambda(\widetilde{\mathbf{v}}_0) = \mathbf{v}_0$, and $D\Phi^\lambda(\widetilde{\mathbf{v}}_1) = \mathbf{v}_1$, where $D\Phi^\lambda$ denotes the derivative mapping of Φ^λ. Let $u_0 = (-v_{12}/v_{13}) \pm \sqrt{1 + (-v_{12}/v_{13})^2}$ and $\lambda = 3/(u_0^3 + 3u_0)$; then for each parametrization Φ^λ of the s-Enneper surfaces satisfying H_C^1, we have that $\Phi^\lambda(0,0) = (0,0,0)$ and $\Phi^\lambda(u_0, 0) = (1,0,0)$ as shown in the proof of Theorem 9. Next, assume that $\widetilde{\mathbf{v}}_0 = (\widetilde{v}_{01}, \widetilde{v}_{02})$ and $\widetilde{\mathbf{v}}_1 = (\widetilde{v}_{11}, \widetilde{v}_{12})$. Then, since

$$\begin{aligned}D\Phi^\lambda(\widetilde{\mathbf{v}}_0) &= \widetilde{v}_{01}D\Phi^\lambda(1,0) + \widetilde{v}_{02}D\Phi^\lambda(0,1)\\&= \widetilde{v}_{01}\Phi_u^\lambda(0,0) + \widetilde{v}_{02}\Phi_v^\lambda(0,0),\\D\Phi^\lambda(\widetilde{\mathbf{v}}_1) &= \widetilde{v}_{11}D\Phi^\lambda(1,0) + \widetilde{v}_{12}D\Phi^\lambda(0,1)\\&= \widetilde{v}_{11}\Phi_u^\lambda(u_0, 0) + \widetilde{v}_{12}\Phi_v^\lambda(u_0, 0),\end{aligned} \quad (20)$$
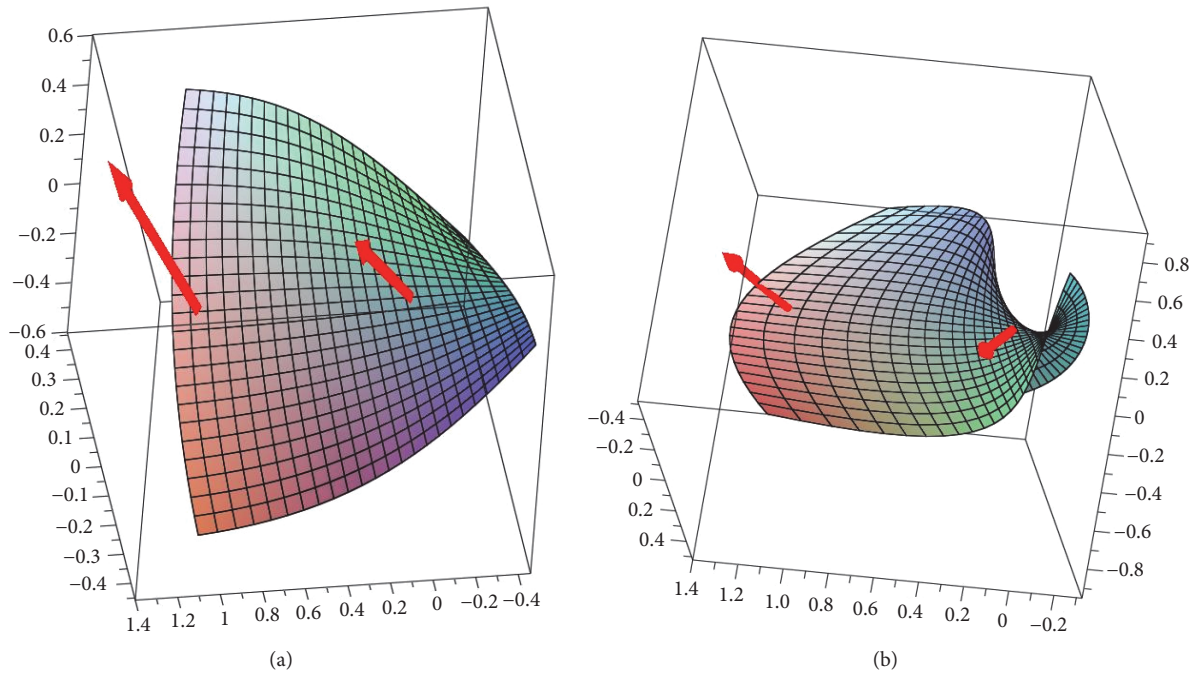
FIGURE 2: Two s-Enneper surfaces satisfying H_C^1 in Example 11: (a) the s-Enneper surface Σ_1^λ that satisfies H_C^1 when $u_0 = (-1 + \sqrt{5})/2$ and $\lambda = (21 + 15\sqrt{5})/38$; and (b) the s-Enneper surface Σ_2^λ that satisfies H_C^1 when $u_0 = (-1 - \sqrt{5})/2$ and $\lambda = (21 - 15\sqrt{5})/38$.

solving simultaneously $D\Phi^\lambda(\widetilde{\mathbf{v}}_0) = \mathbf{v}_0 = (v_{01}, v_{02}, 0)$ and $D\Phi^\lambda(\widetilde{\mathbf{v}}_1) = \mathbf{v}_1 = (v_{11}, v_{12}, v_{13})$ with respect to $\widetilde{v}_{01}, \widetilde{v}_{02}, \widetilde{v}_{12}$ and $\widetilde{v}_{22}$, we obtain

$$\widetilde{v}_{01} = \frac{v_{01}}{\lambda},$$

$$\widetilde{v}_{02} = \frac{v_{02}}{\lambda}, \tag{21}$$

$$\widetilde{v}_{11} = \frac{v_{11}}{\lambda \left(u_0^2 + 1\right)},$$

$$\widetilde{v}_{12} = \frac{v_{13}}{2\lambda u_0}. \tag{22}$$

Finally, we solve the C^1 Hermite interpolation problem for the reduced data-set $\widetilde{H}_C^1$ with planar PH quintics in $\mathbb{R}^2$. Note that if the given data-set H_C^1 is regular, then the reduced data-set $\widetilde{H}_C^1$ is also regular, since Φ^λ is conformal (i.e., angle-preserving). For the regular C^1 Hermite data-set $\widetilde{H}_C^1$, we can always [10] find four interpolants: two of them are simple and the others are loops. Therefore, since Φ^λ is PH-preserving, if $\mathbf{r}$ is a PH interpolant satisfying $\widetilde{H}_C^1$, then $\Phi^\lambda(\mathbf{r})$ is also a PH interpolant satisfying the given data-set H_C^1, which lies on the s-Enneper surface with the parametrization Φ^λ. Consequently, we can obtain four PH interpolants satisfying H_C^1 on each of the two s-Enneper surfaces which satisfy the data-set. Moreover, since Φ^λ is conformal, the topological property of each interpolant on the s-Enneper surface, whether it is a simple curve or a loop, is the same as that of the preimage of itself obtained from the inverse of Φ^λ. This completes the proof. □

Example 13. Let H_C^1 be the same C^1 Hermite data-set as in Example 11. Then, by Theorem 12, we can obtain eight interpolants on the two s-Enneper surfaces which satisfy H_C^1, as shown in Figure 3. They consist of four interpolants on the s-Enneper surface Σ_1^λ, with $u_0 = (-1 + \sqrt{5})/2$ and $\lambda = (21 + 15\sqrt{5})/38$, as shown in Figure 3(b), and four interpolants on the s-Enneper surface Σ_2^λ, with $u_0 = (-1 - \sqrt{5})/2$ and $\lambda = (21 - 15\sqrt{5})/38$, as shown in Figure 3(d). These eight interpolants are obtained from the images of the corresponding planar interpolants, shown in Figures 3(a) and 3(c), which satisfy the reduced data-sets $\widetilde{H}_{C_j}^1$ obtained by the parametrization of each s-Enneper surface Σ_j^λ where $j = 1, 2$.

Corollary 14. *For an arbitrary regular C^1 Hermite data-set $H_C^1 = \{\mathbf{p}_0, \mathbf{p}_1, \mathbf{v}_0, \mathbf{v}_1\}$ in $\mathbb{R}^3$, we can obtain eight interpolants on the surfaces that satisfy H_C^1, by scaling and exploiting the isometry of the two s-Enneper surfaces.*

Proof. Let Ψ be an affine mapping in $\mathbb{R}^3$, obtained by composing a translation, an orthogonal transformation, and a scaling, as shown in Example 3, so that $\Psi(\mathbf{p}_0) = (0, 0, 0)$ and $\Psi(\mathbf{p}_0) = (1, 0, 0)$. Then, using Ψ, we can obtain a new regular C^1 Hermite data-set H_C^{1*} as follows:

$$H_C^{1*} = \{\Psi(\mathbf{p}_0) = (0, 0, 0), \Psi(\mathbf{p}_0) = (1, 0, 0), \sigma\mathbf{R}\mathbf{v}_0, \sigma\mathbf{R}\mathbf{v}_1\}, \tag{23}$$

where σ and $\mathbf{R}$ are, respectively, the scaling factor and the orthogonal matrix of Ψ. Here we can use Theorem 12 to obtain eight interpolants on two s-Enneper surfaces satisfying H_C^{1*}.
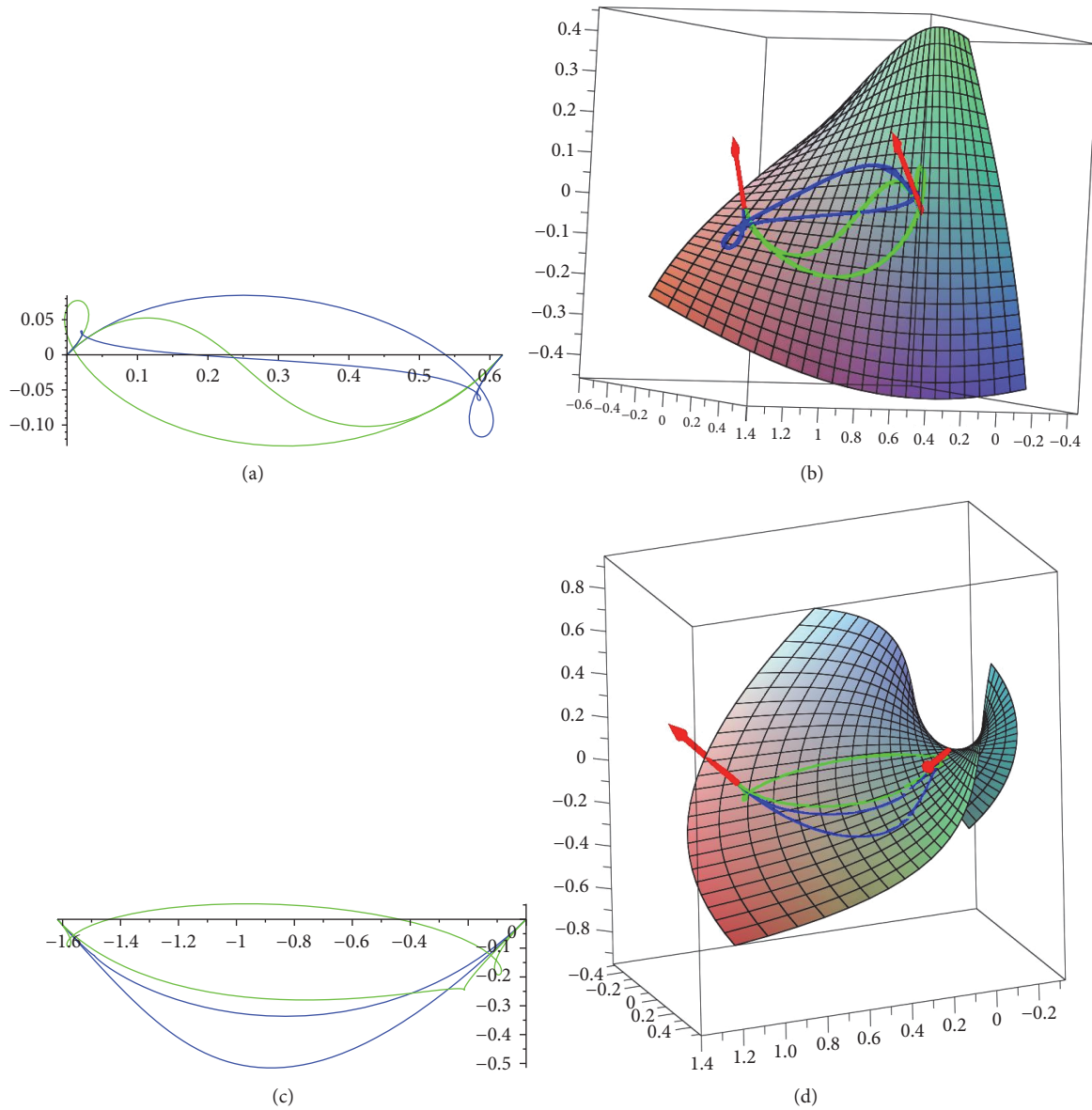
(a)

(b)

(c)

(d)

FIGURE 3: Two s-Enneper surfaces and interpolants satisfying H_C^1 and $\widetilde{H}_{C_j}^1$ ($j = 1, 2$) in Example 13: (a) four interpolants satisfying $\widetilde{H}_{C_1}^1$; (b) four interpolants satisfying H_C^1 on Σ_1^λ; (c) four interpolants satisfying $\widetilde{H}_{C_2}^1$; (d) four interpolants satisfying H_C^1 on Σ_2^λ.

In addition, as shown in Example 3, since Ψ is PH-preserving, we can obtain eight interpolants on the cubic surfaces given by $\Psi^{-1}(\Sigma_j^\lambda)$, where Σ_j^λ is the s-Enneper surface satisfying H_C^{1*}, for $j = 1, 2$. $\qquad\square$

Example 15. Let $H_C^1 = \{\mathbf{p}_0 = (0, 0, 0), \mathbf{p}_1 = (1, 1, 1), \mathbf{v}_0 = (-1, 1, 1), \mathbf{v}_1 = (-1, 0, 1)\}$. Then, as stated in Corollary 14, using the orthogonal matrix $\mathbf{R}$ given by

$$\sigma\mathbf{R} = \begin{pmatrix} \dfrac{1}{3} & \dfrac{1}{3} & \dfrac{1}{3} \\ -\dfrac{\sqrt{2}}{3} & \dfrac{\sqrt{2}}{6} & \dfrac{\sqrt{2}}{6} \\ 0 & -\dfrac{\sqrt{6}}{6} & \dfrac{\sqrt{6}}{6} \end{pmatrix} \qquad (24)$$

with the scaling factor $\sigma = 1/\sqrt{3}$, we can reduce the given data-set to the C^1 Hermite data-set $H_C^{1*} = \{(0, 0, 0), (1, 0, 0), \sigma\mathbf{R}\mathbf{v}_0 = (1/3, 2\sqrt{2}/3, 0), \sigma\mathbf{R}\mathbf{v}_1 = (0, \sqrt{2}/2, \sqrt{6}/6)\}$.

By Theorems 9 and 12, we can obtain two s-Enneper surfaces and eight interpolants satisfying H_C^{1*}. So, using the inverse transformation $\Psi^{-1} = \sigma^{-1}\mathbf{R}^{-1}$ for the surfaces and interpolants, we finally obtain two cubic surfaces and interpolants satisfying the original data-set H_C^1, as shown in Figure 4: The cubic surface and the interpolants shown in Figure 4(b) are obtained by the inverse transformation $\Psi^{-1}(\Sigma_1^\lambda)$, where Σ_1^λ is the s-Enneper surface obtained when $u_0 = 2 - \sqrt{3}$ and $\lambda = (48 + 27\sqrt{3})/26$; and the cubic surface and the interpolants in Figure 4(d) are
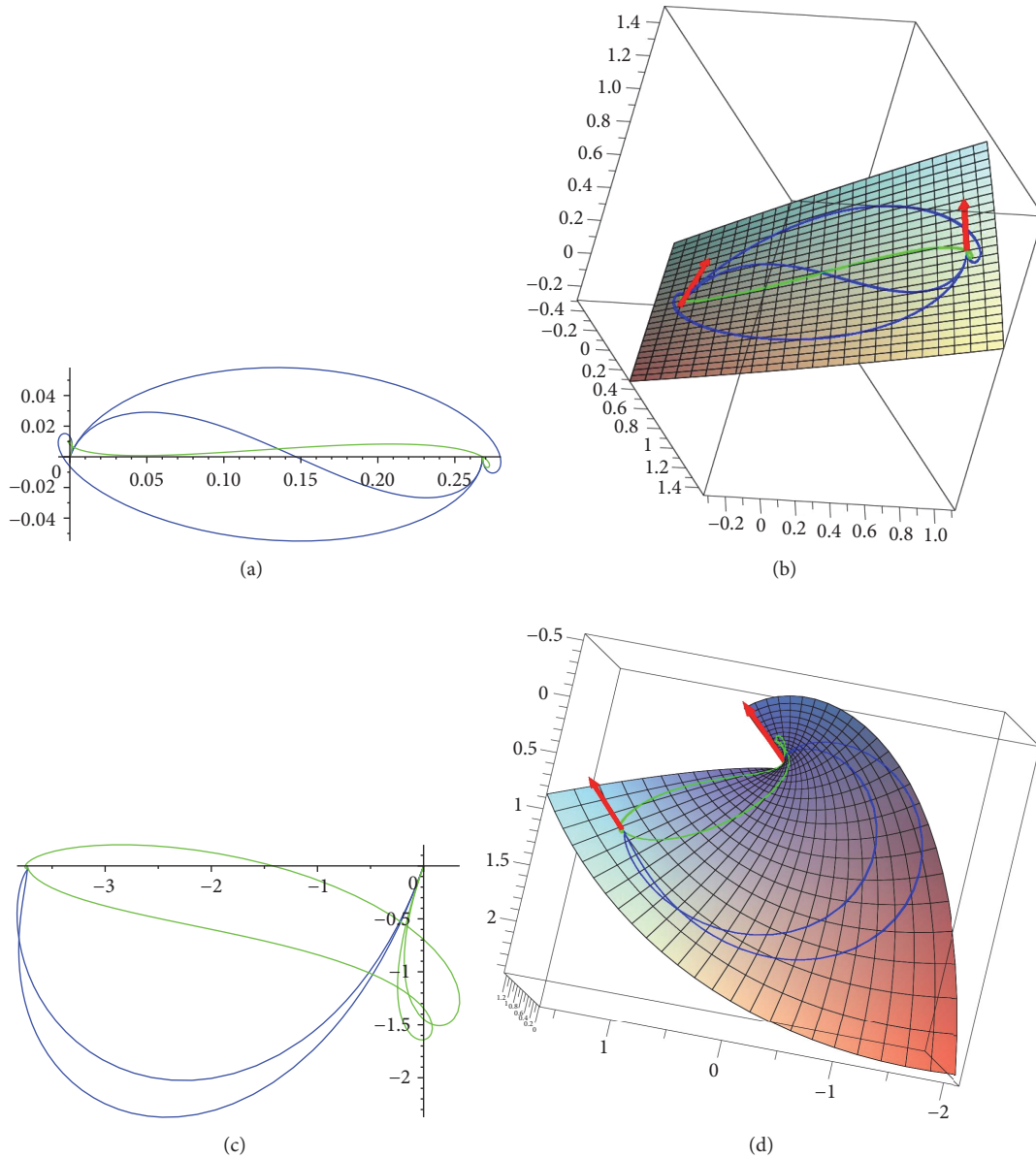
FIGURE 4: The s-Enneper surfaces and interpolants that satisfy H_C^1 in Example 15: (a) four planar interpolants when $u_0 = 2 - \sqrt{3}$ and $\lambda = (48 + 27\sqrt{3})/26$; (b) four interpolants satisfying H_C^1 on the cubic surface $\Psi^{-1}(\Sigma_1^\lambda)$; (c) four planar interpolants when $u_0 = -2 - \sqrt{3}$ and $\lambda = -(48 + 27\sqrt{3})/26$; (d) four interpolants satisfying H_C^1 on the cubic surface $\Psi^{-1}(\Sigma_2^\lambda)$.

obtained by $\Psi^{-1}(\Sigma_2^\lambda)$, where Σ_2^λ is the s-Enneper surface obtained when $u_0 = -2 - \sqrt{3}$ and $\lambda = (-48 + 27\sqrt{3})/26$.

Remark 16. Note that when the given data-set H_C^1 is not regular, that is, $\mathbf{p}_1 - \mathbf{p}_0$, $\mathbf{v}_0$ and $\mathbf{v}_1$ are linearly dependent, these three vectors must lie on a plane in $\mathbb{R}^3$. That allows us to reduce this interpolation problem to a planar C^1 Hermite interpolation problem using a suitable PH-preserving affine transformation. Thus we can obtain [10] four planar PH interpolants satisfying H_C^1.

4. Comparison with Interpolants Obtained by Other PH-Preserving Mappings

In this section, we compare our method with the use of PH-preserving cubic mappings [24]. First note that, for a regular C^1 Hermite data-set H_C^1 in $\mathbb{R}^3$, we can use mappings to obtain 16 interpolants satisfying H_C^1, which consist of four interpolants on each of four cubic surfaces satisfying H_C^1, as shown in Figure 5(a). Whereas, applying our method to the same data-set, we can obtain eight interpolants satisfying H_C^1, which consist of four interpolants on each of two cubic surfaces satisfying H_C^1, as shown in Figure 5(b). Now we will
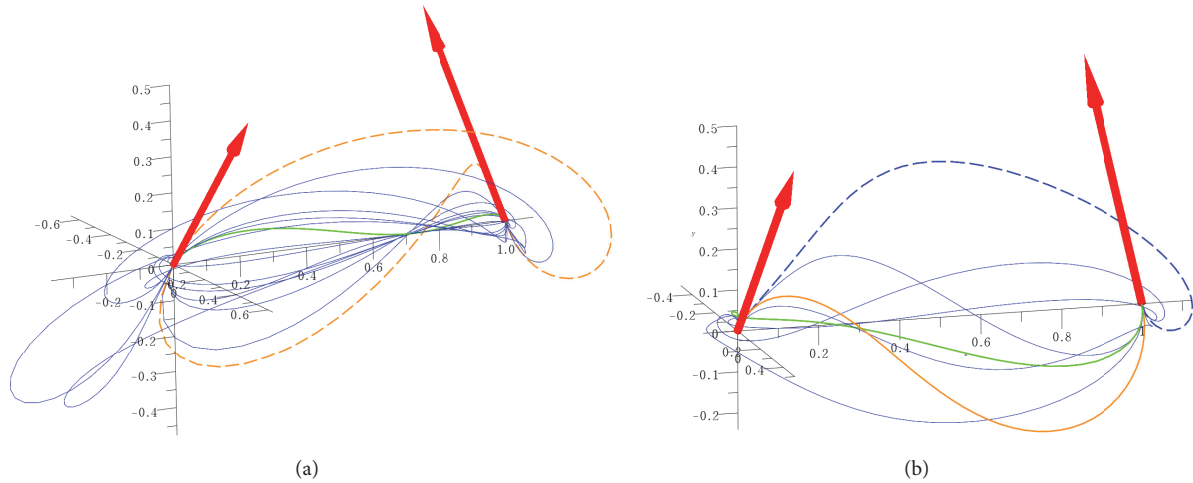
(a)   (b)

FIGURE 5: Comparison of interpolants satisfying $H_C^1 = \{\mathbf{p}_0 = (0, 0, 0), \ \mathbf{p}_1 = (1, 0, 0), \ \mathbf{v}_0 = (0, 1, 1), \ \mathbf{v}_1 = (0, 1, -1)\}$ of Example 11 in [24]: (a) 16 interpolants obtained by using general PH-preserving cubic mappings; (b) 8 interpolants obtained using the s-Enneper surface. In each subfigure, the interpolant with the lowest bending energy is shown as the orange curve; the shortest interpolant is shown as the green curve; and the longest interpolant is shown as the curve denoted by dashed lines.

compare these two methods in terms of their requirements for algebraic computation and the geometries of the resulting curves.

Our method requires less algebraic computation to determine the cubic surfaces satisfying the given data-set than the mapping method: when using the mapping method, to determine the PH-preserving surfaces satisfying the given data-set, lengthy computation processes are additionally required in fixing the free parameters of the surfaces, since they have many free parameters with complicated constraints unlike Enneper surfaces. Moreover, our method only requires the given data-set to meet the regularity condition, whereas mapping requires a data-set which meets several conditions.

We will now examine the shapes of the interpolants produced by mapping and by our method. Looking at the interpolants in Figure 5, it is clear that those in Figure 5(a) are longer and more complicated than those in Figure 5(b), which means that the surfaces satisfying the given data-set H_C^1 must be different.

Next, we will compare the interpolants obtained using each method in terms of bending energy:

$$\mathscr{E}(\gamma) = \int_\gamma \left(\kappa^2 + \tau^2 \right) ds, \tag{25}$$

where κ and τ are the curvature and torsion of an interpolant γ. The bending energy $\mathscr{E}$ of a curve is an established measure of its fairness. We can consider an interpolant to have a better shape than another if it has lower bending energy with a similar arc-length. If we look at the bending energies and arc-lengths in Tables 1 and 2, we observe the following:

(i) While the curve with the lowest bending energy in Figure 5(a) has the longest arc-length, which is about twice that of the shortest curve, the curve with the lowest bending energy in Figure 5(b) is not much longer than the shortest curve.

TABLE 1: Comparison of the bending energies and arc-length of the 3 important interpolants shown in Figure 5(a).

Curve	Bending energy	Arc-length
Dashed-orange 1	**37.308**	2.306
Dashed-orange 2	**37.308**	2.306
Green	153.924	**1.228**

TABLE 2: Comparison of the bending energies and arc-lengths of the 3 important interpolants shown in Figure 5(b).

Curve	Bending energy	Arc-length
Orange	**23.378**	1.609
Green	599.572	**1.251**
Dashed-blue	71.977	**1.805**

(ii) The diversity of arc-lengths among the curves in Figure 5(a) is much larger than the diversity of those in Figure 5(b), where the lengths of the shortest and longest curves are in the ratio 1 : 2.36.

(iii) Finally, the lowest bending energy of any curve in Figure 5(b) is 63% lower than that of the curve with the lowest bending energy in Figure 5(a).

These results suggest that our method can produce better interpolants through a more convenient and shorter algebraic computation than mapping.

5. Concluding Remarks and Suggestions for Further Study

We have proved that the parametrization of the Enneper surface in standard form is PH-preserving and that it also preserves the x- and y-axes in the parametric plane. We went

on to show how to produce interpolants which lie on two s-Enneper surfaces and satisfy a regular C^1 Hermite data-set in $\mathbb{R}^3$. We also proved that eight interpolants can be obtained, four on each of the surfaces. We also compared our method with a previous method [24] based on PH-preserving cubic mappings and showed that we can obtain interpolants with lower bending energy without significant increase in arclength.

The work reported in this paper raises further questions: first, as shown in Section 4, by using different parameterizations to solve the C^1 Hermite interpolation problem satisfying a single data-set H_C^1, we obtain different cubic surfaces. Then the Enneper surface is a minimal surface: does that mean that all the cubic PH-preserving mappings are harmonic? Further, are the surfaces produced by the cubic PH-preserving mappings used in the mapping method also minimal? This brings us to the question of how to characterize all possible cubic PH-preserving mappings. Now, as shown in Example 3 of [24], PH-preserving mappings are not necessarily harmonic; and so PH-preserving surfaces need not to be minimal.

Extending our perspective to include PH-preserving mappings raises another question which brings us nearer to core of the PH-preserving property: what is the key to the property of PH preservation: conformality, harmonicity, or both? finally, we might consider the following interesting questions: can we design new PH-preserving mappings by using specific PH curves in $\mathbb{R}^2$ such as PH-cuts of Laurent series [27]? We have been considering these last two questions and currently believe that the PH-preserving property of mappings is mainly dependent upon conformality. We have to be in a position to write on this topic shortly. In addition, PH and MPH curves are tightly connected, as stated in [11]. Hence, considering our recent work [13] on MPH-preserving mappings, we also naturally reach the following questions: what would be the equivalent of Enneper surfaces in the Minkowski setting? Can we again achieve C^1 interpolation, but this time with MPH curves? These could also be the nice themes for further study.

Conflicts of Interest

The authors declare that they have no conflicts of interest.

Acknowledgments

References

[1] R. T. Farouki and T. Sakkalis, "Pythagorean hodographs," *International Business Machines Journal of Research and Development*, vol. 34, no. 5, pp. 736–752, 1990.

[2] R. T. Farouki, "Pythagorean-hodograph curves in practical use," in *Geometric Processing for Design and Manufacturing*, R. E. Barnhill, Ed., pp. 3–33, SIAM, 1992.

[3] R. T. Farouki, *Pythagorean-Hodograph Curves: Algebra and Geometry Inseparable*, Springer, Berlin, Germany, 2008.

[4] R. T. Farouki, J. Manjunathaiah, D. Nicholas, G.-F. Yuan, and S. Jee, "Variable-feedrate CNC interpolators for constant material removal rates along Pythagorean-hodograph curves," *Computer-Aided Design*, vol. 30, no. 8, pp. 631–640, 1998.

[5] J. Kosinka and M. Lavicka, "Pythagorean hodograph curves: a survey of recent advances," *Journal for Geometry and Graphics*, vol. 18, no. 1, pp. 23–43, 2014.

[6] H. Pottmann, "Rational curves and surfaces with rational offsets," *Computer Aided Geometric Design*, vol. 12, no. 2, pp. 175–192, 1995.

[7] G. Albrecht and R. T. Farouki, "Construction of C^2 Pythagorean-hodograph interpolating splines by the homotopy method," *Advances in Computational Mathematics*, vol. 5, no. 4, pp. 417–442, 1996.

[8] H. I. Choi, D. S. Lee, and H. P. Moon, "Clifford algebra, spin representation, and rational parameterization of curves and surfaces," *Advances in Computational Mathematics*, vol. 17, no. 1-2, pp. 5–48, 2002.

[9] R. T. Farouki, "The conformal map $z \to z2$ of the hodograph plane," *Computer Aided Geometric Design*, vol. 11, no. 4, pp. 363–390, 1994.

[10] R. T. Farouki and C. A. Neff, "Hermite interpolation by Pythagorean hodograph quintics," *Mathematics of Computation*, vol. 64, no. 212, pp. 1589–1609, 1995.

[11] H. P. Moon, "Minkowski Pythagorean hodographs," *Computer Aided Geometric Design*, vol. 16, no. 8, pp. 739–753, 1999.

[12] H. I. Choi, S. W. Choi, and H. P. Moon, "Mathematical theory of medial axis transform," *Pacific Journal of Mathematics*, vol. 181, no. 1, pp. 57–88, 1997.

[13] J. H. Kong, S. Lee, and G. Kim, "Minkowski Pythagorean-hodograph preserving mappings," *Journal of Computational and Applied Mathematics*, vol. 308, pp. 166–176, 2016.

[14] J. Kosinka and B. Jüttler, "C^1 Hermite interpolation by Pythagorean hodograph quintics in Minkowski space," *Advances in Computational Mathematics*, vol. 30, no. 2, pp. 123–140, 2009.

[15] H. I. Choi, R. T. Farouki, S.-H. Kwon, and H. P. Moon, "Topological criterion for selection of quintic Pythagorean-hodograph Hermite interpolants," *Computer Aided Geometric Design*, vol. 25, no. 6, pp. 411–433, 2008.

[16] S. Lee, H. C. Lee, M. R. Lee, S. Jeong, and G.-I. Kim, "Hermite interpolation using Möbius transformations of planar Pythagorean-hodograph cubics," *Abstract and Applied Analysis*, vol. 2012, Article ID 560246, 15 pages, 2012.

[17] R. T. Farouki, M. Al-Kandari, and T. Sakkalis, "Hermite interpolation by rotation-invariant spatial Pythagorean-hodograph curves," *Advances in Computational Mathematics*, vol. 17, no. 4, pp. 369–383, 2002.

[18] R. T. Farouki and T. Sakkalis, "Pythagorean-hodograph space curves," *Advances in Computational Mathematics*, vol. 2, no. 1, pp. 41–66, 1994.

[19] G.-I. Kim, J.-H. Kong, and S. Lee, "First order Hermite interpolation with spherical Pythagorean-hodograph curves," *Journal of Applied Mathematics & Computing*, vol. 23, no. 1-2, pp. 73–86, 2007.

[20] F. Pelosi, R. T. Farouki, C. Manni, and A. Sestini, "Geometric Hermite interpolation by spatial Pythagorean-hodograph cubics," *Advances in Computational Mathematics*, vol. 22, no. 4, pp. 325–352, 2005.

[21] A. Sestini, L. Landolfi, and C. Manni, "On the approximation order of a space data-dependent PH quintic Hermite interpolation scheme," *Computer Aided Geometric Design*, vol. 30, no. 1, pp. 148–158, 2013.

[22] Z. Habib and M. Sakai, "G^2 Pythagorean hodograph quintic transition between two circles with shape control," *Computer Aided Geometric Design*, vol. 24, no. 5, pp. 252–266, 2007.

[23] D. S. Meek and D. J. Walton, "Geometric Hermite interpolation with Tschirnhausen cubics," *Journal of Computational and Applied Mathematics*, vol. 81, no. 2, pp. 299–309, 1997.

[24] G.-I. Kim and S. Lee, "Pythagorean-hodograph preserving mappings," *Journal of Computational and Applied Mathematics*, vol. 216, no. 1, pp. 217–226, 2008.

[25] J. H. Kong, S. P. Jeong, S. Lee, and G. I. Kim, "C^1 Hermite interpolation with simple planar PH curves by speed reparametrization," *Computer Aided Geometric Design*, vol. 25, no. 4-5, pp. 214–229, 2008.

[26] J. H. Kong, H. C. Lee, and G. I. Kim, "C^1 Hermite interpolation with PH curves by boundary data modification," *Journal of Computational and Applied Mathematics*, vol. 248, pp. 47–60, 2013.

[27] H. C. Lee, E. K. Jung, and G. Kim, "Planar C^1 Hermite interpolation with PH cuts of degree (1, 3) of Laurent series," *Computer Aided Geometric Design*, vol. 31, no. 9, pp. 689–700, 2014.

[28] K. Ueda, "Pythagorean-hodograph curves on isothermal surfaces," in *The Mathematics of Surfaces VIII*, pp. 339–353, Information Geometers, 1998.

[29] G. Kim and S. Lee, "Pythagorean-hodograph curves in the Minkowski plane and surfaces of revolution," *Journal of Applied Mathematics & Informatics*, vol. 26, no. 1-2, pp. 121–241, 2008.

[30] J. Kosinka and Z. Sìr, "C^2 Hermite interpolation by Minkowski Pythagorean hodograph curves and medial axis transform approximation," *Computer Aided Geometric Design*, vol. 22, pp. 753–770, 2010.